Reconstruction of Solar Wind Features That Caused a Super Geomagnetic Storm

A. T. Y. Lui[1] and W. D. Gonzalez[2]

[1]JHU/APL, Laurel, MD 20723-6099, USA
[2]INPE, Sao Jose dos Campos, Sao Paulo, Brazil

Abstract. A superstorm with Dst < –300 nT can cause major space disturbances. We examine one on March 31, 2001 that has the minimum Dst of –387 nT and obtain two-dimensional maps in pressure and magnetic field of the sheath region and a magnetic cloud behind it. Both the sheath and the magnetic cloud play a role in building the storm strength. Several properties of the magnetic cloud are inferred, including an estimated total magnetic flux of ~6.5×10^{12} Wb.

Keywords: Superstorm, magnetic cloud, Grad-Shafranov reconstruction.
PACS: 52.25.Xz

INTRODUCTION

The space environment becomes increasingly important for the function of our society due to the growing dependence of our daily lives in space technology. Major space disturbances occur during geomagnetic storms [1-3]. The traditional measure of geomagnetic storm intensity is the Dst index. When this index reaches below –300 nT, it is referred to as a superstorm [3]. Such a superstorm with the Dst reaching –387 nT occurred on March 31, 2001. This superstorm was studied by many for various storm disturbances in the magnetosphere, ionosphere, and thermosphere [4-7].

ACE satellite observed solar wind (SW) features responsible for this superstorm. In order to extend the vision of the SW beyond the one-dimensional measurements from the ACE satellite, we utilize the Grad-Shafranov reconstruction (GSR) technique [8-11] to gain a larger spatial perspective of the event. The results indicate that the SW features consist of filamentary structures in the sheath region with a magnetic cloud (MC) behind them. Both features contributed to the strength of the ensuing superstorm.

ACE OBSERVATIONS

Figure 1 shows the plasma parameters of the SW as observed by the ACE satellite, the Dst index, and the SYM-H index. During this interval, signatures of a MC were seen between 0600-1000 UT. The MC signatures are strong magnetic field, smooth change of magnetic field direction by nearly ~180º, low proton temperature and proton plasma beta [12]. It can be noted that the superstorm started before the arrival of the MC. Furthermore, before 0600 UT, the Dst had already reached –156 nT, almost half of the minimum Dst for this superstorm. This indicates that the sheath region ahead of the MC contributed significantly to the storm strength.

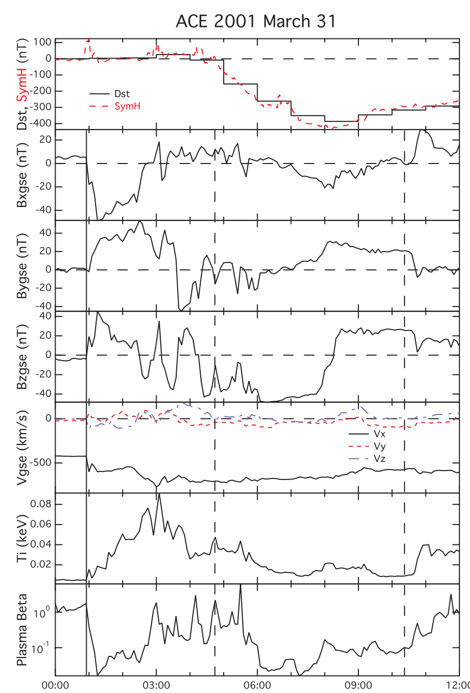

FIGURE 1. The Dst index, SYM-H index (dashed line) and plasma measurements from the ACE spacecraft during the superstorm of March 31, 2001. The three components of the solar wind velocity are given in the *V*gse panel. The ACE data, obtained from OMNI data set in CDAWeb, are time shifted to include the propagation time from the ACE location to the dayside magnetopause. The average time shift for this period is ~33 min.

Solar Wind 13
AIP Conf. Proc. 1539, 406-409 (2013); doi: 10.1063/1.4811071

The SW was at the nominal speed of ~400 km/s before the arrival of the MC and the associated interplanetary shock. The shock front (indicated by the vertical solid line at ~0100 UT) had an initial speed of ~600 km/s and a northward IMF component. Behind this front, the SW speed reached as high as ~700 km/s and the IMF B_z component fluctuated between north and south before becoming mainly southward with the minimum at –48 nT. The IMF B_z component reversed to northward at ~0815 UT for an extended period. The minimum Dst of –387 nT for this superstorm was reached near this sign reversal of IMF B_z, which corresponds to the closest approach to the axis of the MC.

GSR PROCEDURE AND RESULTS

Reconstruction of plasma configuration from observations is based on solving the Grad-Shanfranov (GS) equation with the input of a time series of plasma observations from a single satellite when the structure is two-dimensional (2D) and is in MHD equilibrium. This technique has been discussed in several previous publications [8-11]. The equation is

$$\left(\frac{\partial^2}{\partial x^2}+\frac{\partial^2}{\partial y^2}\right)A=-\mu_0\frac{dP_t(A)}{dA},$$

where the transverse pressure is given by $P_t = P_r + B_z^2/2\mu_0$ and P_r is the plasma pressure. The magnetic field vector **B** is related to the partial vector potential $A(x,y)$ and the axial magnetic field B_z by $\mathrm{B}=\nabla A(x,y)\times\hat{z}+B_z(A)\hat{z}$. The third dimension is considered as the invariant axis, representing the direction along which the structure changes much less than the variation on the plane perpendicular to it. The approach in solving the equation is treating it as a spatial initial value problem. The transverse pressure and the axial magnetic field component B_z are modeled by a combination of polynomial and exponential functions of the partial vector potential $A(x,y)$. For this work, although the fitted values of P_r and B_z are used as initial values for GSR, the model values along the satellite path in the 2D reconstruction maps are interpolated from the solution values on the two adjacent sides of the satellite path. Therefore, the values of these parameters are indeed obtained from the GS solution and not from the fitted curves. Note that high-time resolution (5-min averaged) data are used here in GSR, which leads to more detailed fitting required than those used in previous GSR for MCs, i.e., an improvement over previous attempts [8-10].

The interval of interest is 0450-1020 UT, shown in Figure 1 by the vertical dashed lines. We have verified the appropriateness of the GSR by performing the minimum variance analysis and the deHoffman-Teller (HT) frame transformation. A slightly shorter interval, 0600-1000 UT, is chosen to obtain a better orientation in the GSR of the MC within this interval. The results of these analyses are shown in Figure 2.

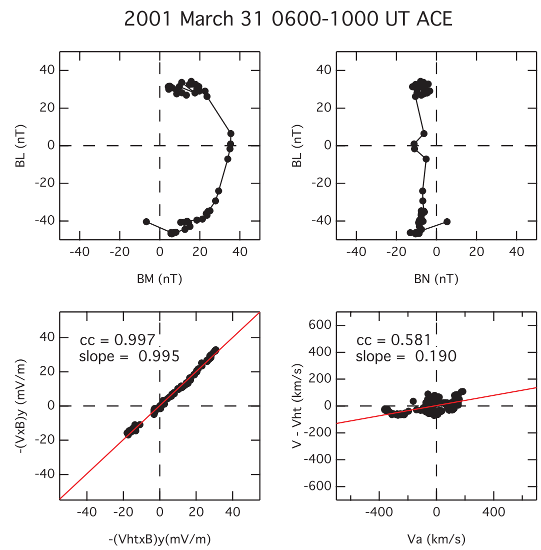

FIGURE 2. The results of minimum variance analysis and the deHoffman-Teller frame transformation.

The minimum, intermediate, and maximum variances are found to be B_N = (–0.690, –0.694, 0.207), B_M = (–0.724, 0.652, –0.226), B_L = (–0.022, 0.306, 0.952), in GSE coordinates, with the eigenvalues of 7.7, 89.3, and 1159, respectively. The eigenvalues indicate well-defined axes. Also, the HT velocity V_{HT} obtained is (–670, 101, –5) km/s. A correlation coefficient of 0.997 between $-(V\mathrm{x}B)_y$ and $-(V_{HT}\mathrm{x}B)_y$ is found with a slope of 0.995±0.007, indicating the existence of a moving frame in which the structure fits well with a relatively steady state condition. The HT result also shows a lack of fast flows in the transformed frame, again consistent with the steady state assumption for the structure. Thus, the observed structures have properties satisfying the requirements for the GSR.

The GSR axes (using R to denote GSR coordinates) are XR = (0.69, 0.69, –0.23), YR = (–0.01, –0.31, –0.95), and ZR = (–0.72, 0.66, –0.21) in GSE coordinates. These axes were obtained through a number of rotations starting from the minimum variance axes to determine the optimal orientation of the axes for reconstruction. One may note that the YR-axis is close to GSE $-Z$-axis, indicating that the extended vision of the SW is mainly in the north-south direction.

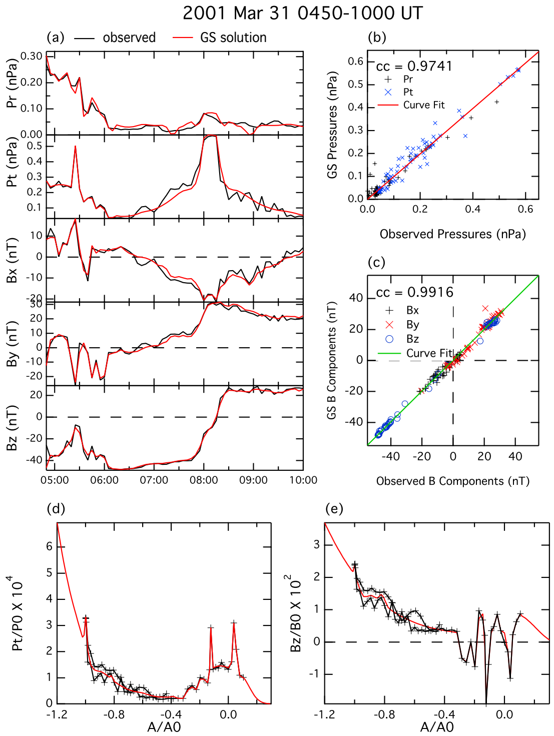

FIGURE 3. (a) Comparison between the observed and GSR values for the pressure and the magnetic field components; (b) a quantitative comparison of pressures between observed and GSR values; (c) a quantitative comparison of magnetic field components between observed and GSR values; (d) a plot to show the observed P_t as a function of $A(x,y)$ and its fitted curve; (e) a plot to show the observed B_z as a function of $A(x,y)$ and its fitted curve.

The accuracy of the reconstruction results can be verified by comparing the observed values of P_t, P_r, and the magnetic field components with the values from the solution values, which are not the fitted values as mentioned earlier. Figure 3a shows the comparison of these parameters, indicating that there are good agreements between the observed values and GS solutions for all these parameters. A quantitative comparison for the transverse and plasma pressures shown in Figure 3b gives a correction coefficient of 0.974 and a slope of 0.968±0.014. Similarly, a quantitative comparison for the magnetic field components shown in Figure 3c gives the correlation coefficient and the slope to be 0.992 and 0.991±0.021, respectively. The values of these parameters are close to unity, indicating very good matches. Figures 3d-3e show, respectively, the observed P_t and B_z and their fitted curve along the satellite path as a function of the normalized $A(x,y)$.

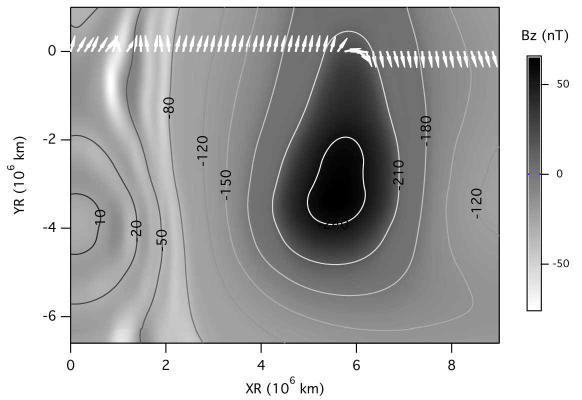

FIGURE 4. A 2D map of the B_z component in GS coordinate system overlaid with contours of $A(x,y)$ and observed magnetic field vectors projected on this GS plane.

Figure 4 shows specifically the GSR of MC within this interval. The color in this 2D map shows the B_z component in the GS coordinate system and the contours are based on $A(x,y)$ values. Overlaid are the observed magnetic field vectors on this plane. From this map, the core of the MC was at ~470 R_E below the GS Y-axis, i.e., above the GSE Z-axis. In front of the MC (on the left side of the panel) were several filamentary structures related to the sheath region with strong and spatially varying magnetic field.

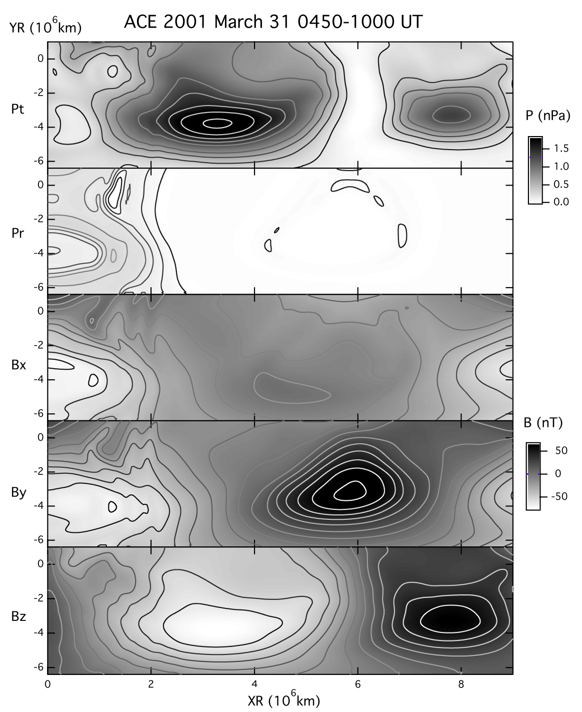

FIGURE 5. Two-dimensional maps obtained from the GSR of the pressures and the magnetic field components in GSE coordinates.

Reconstruction maps of P_t, P_r, and the magnetic field components in GSE coordinates are shown in Figure 5. Note that P_t in GSE coordinates is different from P_t in GS coordinates since it has a term involving B_z in GSE coordinates. From these 2D maps, the filamentary structures in the sheath region can be seen in all these parameters. In particular, the P_t had high values (~0.8 nPa) while P_r had low values (<0.1 nPa) before the arrival of the MC. The most negative GSE B_z was –71 nT. There were significant structures in plasma and field values within the sheath region prior to the MC arrival (on the left side of the panels). There was strong B_y (~83 nT) within the MC and B_z changed sign within the MC as expected for a magnetic flux rope structure.

One can also obtain the total magnetic flux content by summing the magnetic flux threading through the GS plane. If one defines the MC by $A(x,y)$ = –210 T-m, then one obtains the total magnetic flux content of this MC to be $\sim 6.5\times 10^{12}$ Wb. This is probably a conservative estimate with the chosen $A(x,y)$.

SUMMARY AND DISCUSSION

We have examined the solar wind features associated with the superstorm on March 31, 2001 with the Grad-Shafranov reconstruction technique using 5-min averaged plasma measurements from the ACE spacecraft to gain a larger spatial perspective of the solar wind features linked to the superstorm. The reconstruction technique enables us to ascertain plasma parameters of the solar wind not directly measured by the ACE spacecraft. The reconstruction maps indicate that the solar wind features leading to a superstorm at Earth had filamentary structures in plasma and magnetic field parameters for the sheath region ahead of a magnetic cloud. The main core of the magnetic cloud was ~470 R_E above the GSE *XY*-plane, had a minimum B_z in GSE coordinates of about –71 nT, a core magnetic field ~83 nT, and a total magnetic flux content of $\sim 6.5\times 10^{12}$ Wb. It is noted that the Dst reached –157 nT even before the arrival of the magnetic cloud, indicating significant contribution to storm strength by the sheath region.

ACKNOWLEDGMENTS

This work was supported in part by NSF grant ATM-0852508 and NASA grant NNX12AP62G to The Johns Hopkins University Applied Physics Laboratory and in part by the "Fundaçao de Amparo a Pesquisa do Estado de Sao Paulo" of Brazil under project 2008/06650-9.

REFERENCES

1. Kamide, Y., et al., Current understanding of magnetic storms: Storm-substorm relationships, *J. Geophys. Res.*, *103*, 17705-17728, (1998).
2. Tsurutani, B. T., et al., Origin of interplanetary southward magnetic fields responsible for major magnetic storms near solar maximum (1978-1979), *J. Geophys. Res.*, *93*, 8519-8531, (1988).
3. Gonzalez, W.D., et al., Solar and interplanetary causes of very intense geomagnetic storms, *J. Atmos. Sol. Terr. Phys*., 63, 403, (2001).
4. Foster, J. C., et al., Ionospheric signatures of plasmaspheric tails, *Geophys. Res. Lett., 29* (13), (2002).
5. Ober, D. M., M. F. Thomsen, and N. C. Maynard, Observations of magnetopause and bow shock crossings from geosynchronous orbit on March 31, 2001, *J. Geophys. Res.*, *107* (A8), 1206, (2002).
6. Huang, C.-S., et al., Periodic magnetospheric substorms and their relationship with solar wind variations, *J. Geophys. Res.*, *108* (A6), 1255, (2003).
7. Kil, H., et al., Characteristics of the storm-induced big bubbles (SIBBs), *J. Geophys. Res., 111*, A10308, (2006).
8. Sonnerup, B. U. Ö and M. Guo, Magnetopause transects, *Geophys. Res. Lett.*, *23*, 3679-3682 (1996).
9. Hau, L.-N. and B. U. Ö Sonnerup, Two-dimensional coherent structures in the magnetopause: Recovery of static equilibria from single-spacecraft data, *J. Geophys. Res*., *104*, 6899-6917 (1999).
10. Hasegawa, H., et al., Reconstruction of two-dimensional magnetopause structures from Cluster observations: verification of method, *Ann. Geophys*, *22*, 1251-1266 (2004).
11. Lui, A. T. Y., Grad-Shafranov reconstruction of magnetic flux ropes in the near-Earth space, *Space Sci. Rev*., *158*, 43-68, (2011).
12. Burlaga, L. F., *Interplanetary Magnetohydrodynamics*, p. 91, Oxford Univ. Press, New York, (1995).